Tarım Bilimleri Dergisi
Tar. Bil. Der.
Dergi web sayfası:
www.agri.ankara.edu.tr/dergi

Journal of Agricultural Sciences
Journal homepage:
www.agri.ankara.edu.tr/journal

Kinematics Analysis and Simulation of A 5DOF Articulated Robotic Arm Applied to Heavy Products Harvesting

Ali ROSHANIANFARD[a], Noboru NOGUCHI[a]

[a]*Hokkaido University, Graduate School of Agriculture, Laboratory of Vehicle Robotics, Kita-9, Nishi-9, Kita-ku, Sapporo 060-8589, JAPAN*

ARTICLE INFO
Research Article DOI: 10.15832/ankutbd.446396
Corresponding Author: Noboru NOGUCHI, E-mail: noguchi@cen.agr.hokudai.ac.jp, Tel: +81 (90) 88 955 835
Received: 15 June 2016, Received in Revised Form: 18 August 2017, Accepted: 17 September 2017

ABSTRACT

Robotics can play a significant role to increase efficiency and lighten the farmer's load. Despite challenges in the agricultural robotic designs, robots are capable of performing various tasks and changing themselves accordingly, based on specific conditions. To address modern problems in the agricultural field, an agricultural robot is one of the key technologies. Although agricultural robotic is still in the development stage, robots have a bright future ahead. This paper proposes a new 5DOF articulated robotic arm design that would become a solution for heavy crop harvestings like pumpkin and cabbage. After the development stage, this robotic arm will be mounted on a robot tractor for real experimentation.

The main design process of this robotic arm was conceived using 6 stages of Shigley design process. All components were designed, assembled and analyzed by using Solidworks 2014 in compliance with Japanese Industrial Standards (JIS) standards. The parts of the system that had dynamic nature were analyzed manually using standard mechanical formulas. Calculations of the workspace required joint torque, and coordination of mass center position was done by using standard machine design methods. Denavit-Hartenberg method was used to calculate forward and inverse kinematics. To resolve the torque reduction, components were designed using different materials and mass centers and comparing their performance.

Results showed that total torque in Joints number 1, 2, 3, 4 and 5 were 6.15, 257.35, 103.4, 20.2 and 0.1 respectively with a rotational speed range of 15 ~ 60 rpm. Changes in the linkage material and servo motor location improved 29.7% ~ 47.7% and 29.7% ~ 68.9% of the total required torque for each joint. The maximum distance covered by the arm was 1421 mm from the and 2026 mm from the attachment point. According to the feedback received from a inverse kinematics equation algorithm, the fundamental operation of the robot arm had an optimal performance.

Keywords: Forward kinematics; Inverse kinematics; Torque; Workspace; Servo motor

Ağır Ürünlerin Hasadında Kullanılan Bir 5DOF Eklemli Robot Kolun Kinematik Analizi ve Simülasyonu

ESER BİLGİ:
Araştırma Makalesi
Sorumlu Yazar: Noboru NOGUCHI, E-posta: noguchi@cen.agr.hokudai.ac.jp, Tel: Tel: +81 (90) 88 955 835
Geliş Tarihi: 15 Haziran 2016, Düzeltmelerin Gelişi: 18 Ağustos 2017, Kabul: 17 Eylül 2017

ÖZET

Robotlar etkinliği artırmak ve çiftçilerin yükünü hafifletmekte önemli bir rol oynayabilir. Tarımsal amaçlı robot dizaynlarındaki zorluklara rağmen, robotlar çeşitli görevleri yerine getirmede ve kendilerini duruma göre değiştirmede belli koşullara göre kabiliyetlidirler. Tarım alanındaki modern problemlerin ifade edilmesinde, bir tarımsal robot anahtar teknolojilerden biridir. Tarımsal robotlar halen gelişme aşamasında olmalarına rağmen, robotlar parlak bir geleceğe sahiptirler. Bu yayın kabak ve lahana gibi ağır ürünlerin hasadına bir çözüm olabilecek yeni bir 5DOF eklemli robot kol dizaynını sunmaktadır.

Düzeneğin ana dizayn süreci altı aşamalı Shigley dizayn prosesi kullanılarak tasarlanmıştır. Tüm parçaların dizaynı, birleştirilmesi ve analizi JIS standartları ile uyumlu Solidworks 2014 kullanarak gerçekleştirilmiştir. Dinamik yapıda olan sistem parçaları standart mekanik formüllerin kullanılması ile manuel olarak analiz edilmişlerdir. İleri ve geri kinematiklerin hesaplanmasında Denavit-Hartenberg yöntemi kullanılmıştır. Tork azalma problemini ortadan kaldırmak için parçalar farklı materyallerle ve kütle merkezine göre dizayn edilmiştir ve beraber karşılaştırılmıştır.

Sonuçlar göstermiştir ki 1, 2, 3, 4 ve 5 numaralı eklemlerde toplam tork, 15 ~ 60 rpm rasyonel hız aralığı ile sırasıyla 6.15, 257.35, 103.4, 20.2 ve 0.1 olmuştur. Bağlantı materyalindeki ve servo motor lokasyonundaki değişiklikler her bir eklem için olan toplam gerekli torku % 29.7~ % 47.ve % 29.7% ~ % 68.9 aralıklarında iyileştirmiştir. Kol tarafından taranan maksimum mesafe J_2 den 1421 mm ve eklem noktasından da 2026 mm olmuştur. Ters kinematik eşitliği algoritmasından alınan geri beslemeye göre robot kolunun temel operasyonları optimum bir performans göstermiştir.

Anahtar Kelimeler: İleri yönlü kinematik; Ters kinematik; Tork; Çalışma alanı; Servo motor

1. Introduction

In the last three decades, the engineers had a new approach to design particular robots for the agriculture industry. Although it is an important industry, it faces several problems like the age distribution of farmers. The average age of a farmer is 65.9 years old in Japan (MAFF 2016) and 55.9 years old in USA (USDA 2015). With a declining farming population, the majority of the farming population is considered "too old" to handle the rigorous demands of the industry. Not to mention the work itself is susceptible to unpredictable weather conditions. Another issue is utilizing new agricultural technology. Learning how to operate new technology requires time and physical effort. According to the last report of Statistics Bureau of Japan, the number of workers decreased from 13.40 million in 1960 (30.2 percent of the total workforce) to 2.33 million in 2013 (3.7 percent), and the GDP share of the industries fell from 12.8 percent in 1960 to 1.2 percent in 2013. Japan's total agricultural output in 2013 was 8.47 trillion yen, down 0.7 percent from the previous year. Crops yielded 5.70 trillion yen, down 3.0 percent from the previous year. This was due to the rice output decreasing despite outputs of vegetables and fruits and nuts increasing. Based on the Global Agricultural Productivity report, in the next 40 years, agricultural output will need to increase by 100%. Consumer attitudes is changing to organic products and the total income per commercial farm household has decreased. In 2013, the total income per commercial farm household was 4.73 million yen, down 0.7 percent from the previous year. Of that amount, 1.32 million yen was from farming income, 1.53 million yen from non-farming income, and 1.87 million yen from pension benefits and other sources. Agricultural robotics can help address and solve these issues that farming communities encounter on a regular basis (Cassinis & Tampalini 2007). Some example include a multi-arm robotic harvester (Zion et al 2014), a strawberry-harvesting robot (Hayashi et al 2010), an apple harvesting robot (De-An et al 2011), an autonomous robot for white asparagus harvesting (Barawid Jr et al 2007), a cherry-harvesting robot (Tanigaki et al 2008), robots for tomato, petty-tomato, cucumber and grape harvesting (Kondo et al 1996) and Stationary robots that are used for sheep herding (Tanner et al 2001).

To design a robotic arm for agricultural applications, it is necessary to move the final point of a manipulator along some desired path at a prescribed speed (Angeles 1997). Furthermore, it is necessary for the system to be dynamically analyzed and modeled (Wang et al 2003). To reach this goal, it is essential to use forward and inverse kinematics (Karlik & Aydin 2000).

The motion takes place in the Cartesian space; but most of the industrial robots, especially the articulated robotic arm, are controlled in rotary joint spaces. Therefore, a kinematic transformation between the Cartesian space and joint space is needed (Balkan et al 2000). The most widely proposed methods for solving the inverse kinematic problem for redundant manipulators involve the use of the Jacobian pseudoinverse manipulator (Yahya et al 2011). Thanks to this method, many excellent types of research in the kinematics community had been done by the end of the 1980s and the beginning of 1990s. At the same time, resolving of inverse kinematics was considered to be the most difficult task in the field of kinematics. In 1988 Lee & Liang (1988) came up with a solution which was not very transparent, so most of the time the Raghavan & Roth (1990) solution is cited in the literature. There were many attempts to improve the controlling algorithm (Ghazvini 1993). As a result, there are many thousands of robots in the industry (Satoru 2011) but only a few are designed for agriculture application.

The promising results of laboratory investigations can be considered as a cornerstone for the development of models for farming robots. Currently, the agricultural robotic technology is in the development stage, and it is expected that the agricultural robots can cover all the needs of agriculture. However, researchers had not investigated the topic of heavy harvesting crops like cabbage, pumpkin, and watermelon as much as light crops. Since users intend to take advantage of fully automated processes in different aspects of agriculture through the use of robotic technology, further research; especially on harvesting agricultural heavy products is required.

This research presents a new type of 5DOF robotic arm mounted on a tractor for heavy crop harvestings like pumpkin and cabbage.

2. Material and Methods

In this study, a 5DOF (Degrees of Freedom) robotic arm for the harvesting the heavy agricultural products (RAVebots-1/Robotic Arm for Vehicle Robotic) was developed, which is shown schematically in Figure 1. The presented robotic arm is composed of serial links which are affixed to each other with revolute joints from the base frame to the end-effector. The RAVebots-1's structure was chosen to be manufactured for heavy product harvesting application. All components were designed, assembled and analyzed using Solidworks 2014. Dynamic components were analyzed by using standard mechanical formula. After finishing all component development, The RAVebots-1 was attached to a robot tractor.

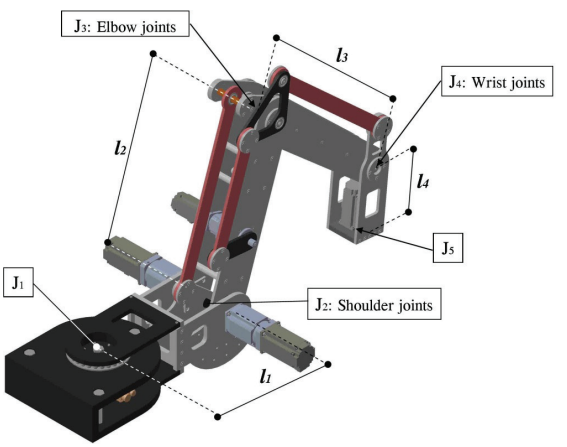

Figure 1- Assembled model of RAVebots-1

2.1. Description of the RAVebots-1 workspace

The robot workspace or reachable spaces consist of all the points in the Cartesian space that the end effector of the robotic arm can access. The workspace and a quick access to a certain point in all robotic arms are strongly dependent on linkages properties, joint properties (length, angles, angular velocity

and torque), DOF, angle/translation limitations, and robot configuration.

Consider the RAVebots-1 in Figure 2. The left side shows the complete work envelope of the robot from the side view. The right side of Figure 2 shows the whole workspace from the top view. The Maximum frontal distance covered by the arm is 1640 mm from and 1830 mm from the robotic arm and tractor's attachment point. The height limitation comes from the tractor height which was almost than 700 mm. All dimensions have a tolerance in the range of 2 ~ 5 mm. The maximum height of access point is 1430 mm. According to the accessible points in X and Z directions, the RAVebots-1 has enough range of motion to be used in horticulture applications. In addition, the RAVebots-1's workspace has a suitable reach to pick fruits; cut branches and perform precision farming.

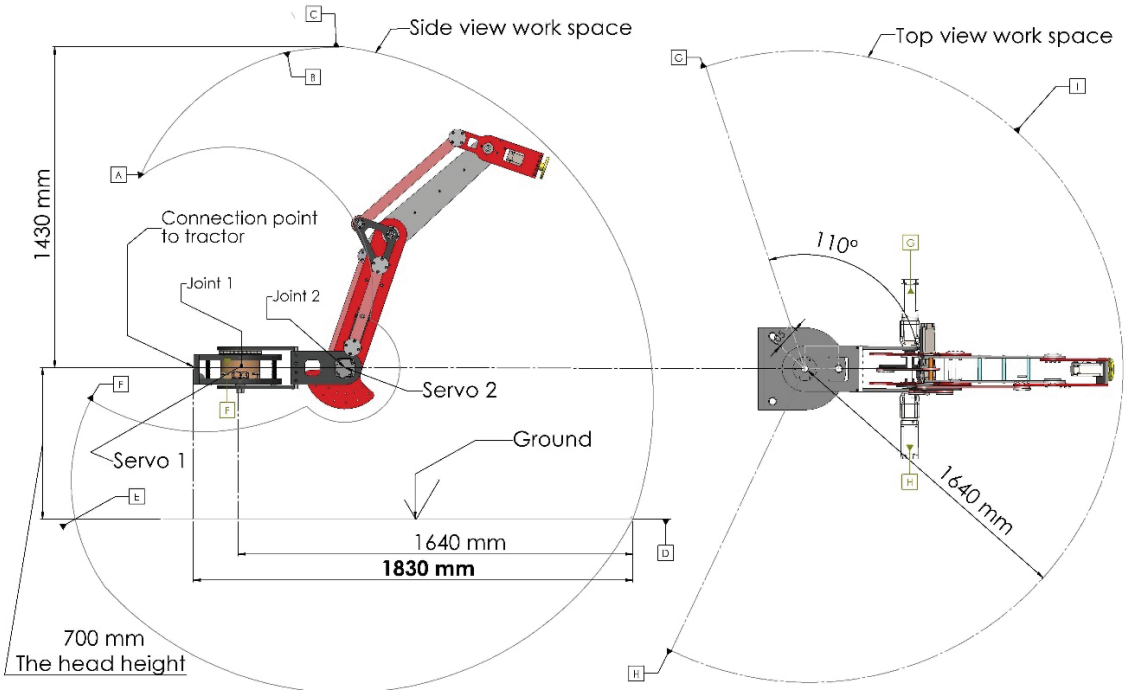

Figure 2- Workspace of the RAVebots-1

2.2. Structural design of RAVebots-1

2.2.1. Components analysis

Figure 3 shows a comparison between three design models of RAVebots-1 (A, B, and C) in terms of different material and structure. Overall, the main differences between A and B designs are related to the material; A used ASTM A36 steel and B used AL5202. The difference between A and B designs with design C relies not only on the material used but also in the servo motor position. A special alloy of Aluminum (AL5202) was used in design C, and the positions of the servo motors from joint 3 and 4 are closer to the position of joint 2.

The dynamic components were analyzed by using standard mechanical formulas. Due to the sensitivity of some parts such as the main chassis, a stress analysis was conducted on joint-1 structure and vertical plates using the

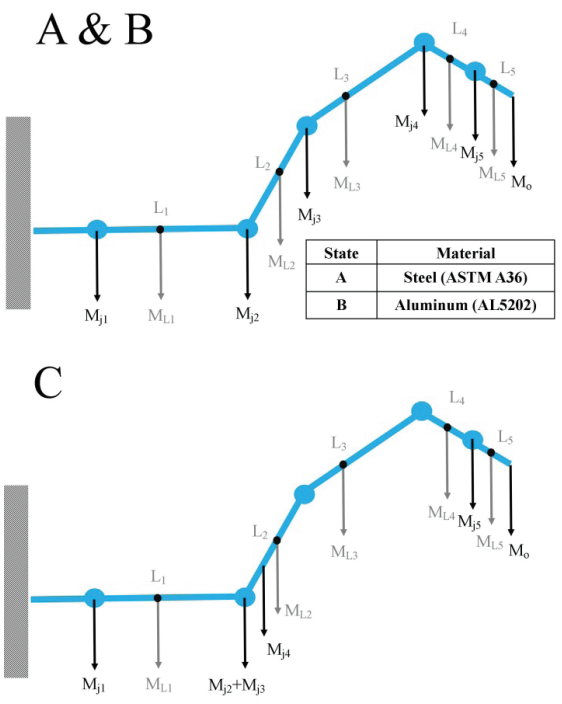

Figure 3- Components weight diagram in A, B, and C design

Solidworks 2014 simulation. The safety factor range for linkage and structure design was selected from 1.96 to 2.60; the range of joint and servo motor designs was selected from 1.1 to 3.00. All components were manufactured from steel (ASTM A36 steel) and aluminum (AL5205). The simulation type of Solidworks simulator was linear elastic isotropic (Richard & Keith 2006). Stress analysis results for the main stage showed that the maximum stress was less than the tensile strength (Figure 4).

2.2.2. Joints torque analysis

Selecting a proper motor and a motor driver to meet a specific application needs a torque calculation. At first, the inertia, friction, and load torque should be calculated. Then, it is possible to determine the required motor torque for the specific application. Finally, it is possible to select the proper motor and driver based on their speed-torque characteristics.

The load drive torque of the servo motor can be calculated by using Equation 1.

$$T_t = \left((I.\omega)+(N.K_i + T_{FM} + T_{FD}) + (T_g + T_s)\right) \times \frac{FOS}{\eta} \qquad (1)$$

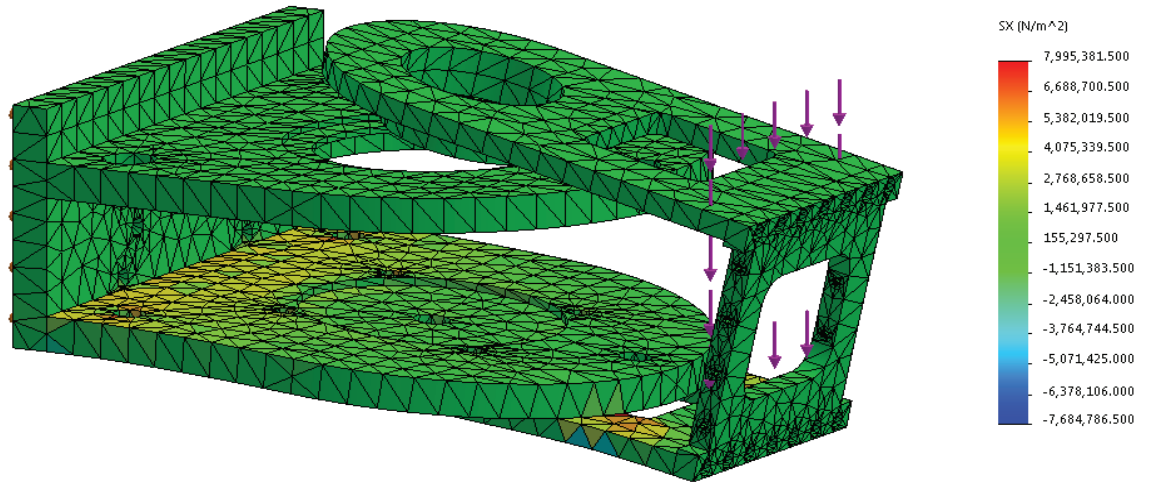

Figure 4- Stress analysis illustration of the main stage by using Solidworks

The symbols of Equation 1 are defined as follow:

Symbol	Meaning	Unit	Symbol	Meaning	Unit
I	Total moment of inertia in conversion into the motor's shaft	Nms^2	T_{FD}	Friction torque of the transmission system	N.m
ω	Motor shaft angular acceleration	$Rads^{-2}$	η	Efficiency of Servo motor	-
N	Motor usage	rpm	FOS	Factor of Safety	-
K_i	Braking constant	Nm/rpm	T_g	Gravity holding torque	N.m
T_{FM}	Motor static friction torque	N.m	T_s	Interference torque	N.m

2.3. Kinematics modeling

Robot kinematics refers to the analytical study of the motion of a robot manipulator. Denavit & Hartenberg (1955) showed that a general transformation between two joints requires four parameters. These parameters, known as the Denavit-Hartenberg (D-H) parameters which became a standard to describe robot kinematics (Funda et al 1990). The robot kinematics can be divided into forward and inverse kinematics (Siciliano & Khatib 2008). Forward kinematics problems are straightforward, with little complexity in driving their respective equations (Craig 1989). Inverse kinematics is more difficult to solve than forward kinematics (Serdar & Zafer 2006; Satoru 2011).

In this section, the analytical solution for the manipulator is examined using the D-H parameter into forward kinematics and inverse kinematics.

2.3.1. Forward kinematics

Forward kinematics problem involves finding the position and orientation of a robot end-effector as a function of its joint angles. Denavit-Hartenberg (D-H) method uses the four parameters including a_{i-1}, α_{i-1}, d_i and θ_i; which are the link length, link twist, link offset and joint angle, respectively. Figure 5 presents the coordinate frame assignment for a general manipulator (Serdar & Zafer 2006).

The matrix T_i^{i-1} is known as a D-H convention matrix given in Equation 2.

$$T_i^{i-1} = \begin{bmatrix} cos\,\theta_i & -cos\,\alpha_{i-1}\,sin\,\theta_i & sin\,\alpha_{i-1}\,sin\,\theta_i & a_{i-1}\,cos\,\theta_i \\ sin\,\theta_i & cos\,\alpha_{i-1}\,cos\,\theta_i & -sin\,\alpha_{i-1}\,cos\,\theta_i. & a_{i-1}\,sin\,\theta_i \\ 0 & sin\,\alpha_{i-1} & cos\,\alpha_{i-1} & d_i \\ 0 & 0 & 0 & 1 \end{bmatrix} \quad (2)$$

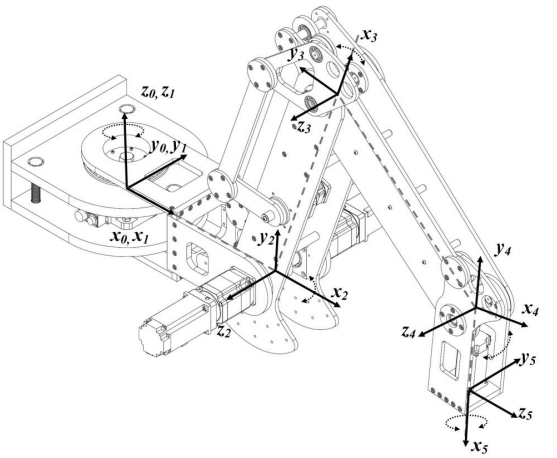

Figure 5- Axis's direction and angle parameters

In the matrix T_i^{i-1}, the quantities of $\alpha_{i-1}, a_{i-1}, d_i$ are constant for a given link while the parameter eter θ_i for a revolute joint is variable. The next step was determining the D-H parameters by using α_i. The completed D-H parameters for RAVebots-1 are listed in Table 1. Using the expression in Equation 2, the A-matrices of each joint can be built as shown in Equation 3.

Table 1- D-H Parameters of a RAVebots-1 Robot

Axis number	*Twist angle* α_{i-1}	*Link length* α_{i-1}	*Link offset* d_i	*Joint angle* θ_i
1	90°	l_1	0	$-105° < \theta_1 < 105°$
2	0	l_2	0	$0 < \theta_2 < 125°$
3	0	l_3	0	$-130° < \theta_3 < -10°$
4	−90°	l_4	0	$-115° < \theta_4 < 0°$
5	*0*	l_5	0	$0° < \theta_5 < 360°$

$$T_1^0 = \begin{bmatrix} cos\,\theta_1 & 0 & sin\,\theta_1 & l_1\,cos\,\theta_1 \\ sin\,\theta_1 & 0 & -cos\,\theta_1 & l_1\,sin\,\theta_1 \\ 0 & 1 & 0 & 0 \\ 0 & 0 & 0 & 1 \end{bmatrix}, T_2^1 = \begin{bmatrix} cos\,\theta_2 & -sin\,\theta_2 & 0 & l_2\,cos\,\theta_2 \\ sin\,\theta_2 & cos\,\theta_2 & 0 & l_2\,sin\,\theta_2 \\ 0 & 0 & 1 & 0 \\ 0 & 0 & 0 & 1 \end{bmatrix}$$

$$T_3^2 = \begin{bmatrix} cos\,\theta_3 & -sin\,\theta_3 & 0 & l_3\,cos\,\theta_3 \\ sin\,\theta_3 & cos\,\theta_3 & 0 & l_3\,sin\,\theta_3 \\ 0 & 0 & 1 & 0 \\ 0 & 0 & 0 & 1 \end{bmatrix}, T_4^3 = \begin{bmatrix} cos\,\theta_4 & 0 & -sin\,\theta_4 & l_4\,cos\,\theta_4 \\ sin\,\theta_4 & 0 & cos\,\theta_4 & l_4\,sin\,\theta_4 \\ 0 & 1 & 0 & 0 \\ 0 & 0 & 0 & 1 \end{bmatrix} \quad (3)$$

$$T_5^4 = \begin{bmatrix} cos\,\theta_5 & -sin\,\theta_5 & 0 & l_5\,cos\,\theta_5 \\ sin\,\theta_5 & cos\,\theta_5 & 0 & l_5\,sin\,\theta_5 \\ 0 & 0 & 1 & 0 \\ 0 & 0 & 0 & 1 \end{bmatrix}$$

The T-matrix is created by multiplying each T_5^0 matrix defined using Equation 3; the result is shown in Equation 4.

$$T_5^0 = \prod_{i=1}^{5} T_i^{i-1} = T_1^0\,T_2^1\,T\,{}_3^2\,T_4^3\,T_5^4 = \begin{bmatrix} r_{11} & r_{12} & r_{13} & r_{14} \\ r_{21} & r_{22} & r_{23} & r_{24} \\ r_{31} & r_{32} & r_{33} & r_{34} \\ r_{41} & r_{42} & r_{43} & r_{44} \end{bmatrix} \quad (4)$$

Where the matrix elements are defined in Equation 5 as:

$$\begin{aligned} &r_{11} = c_1c_{(2+3+4)}c_5 + s_1s_5, r_{12} = s_5\left(s_1 - c_1c_{(2+3+4)}\right), r_{13} = -c_1s_{(2+3+4)} \\ &r_{14} = c_1\left(l_1 + l_2c_2 + l_3c_{(2+3)} + l_4\,c_{(2+3+4)} + l_5c_5c_{(2+3+4)}\right) + l_5s_1s_5 \\ &r_{21} = s_1c_{(2+3+4)}c_5 - c_1s_5, r_{22} = -s_1c_{(2+3+4)}s_5 - c_1c_5, r_{23} = -s_1s_{(2+3+4)} \\ &r_{24} = s_1\left(l_1 + l_2c_2 + l_3c_{(2+3)} + l_4\,c_{(2+3+4)} + l_5c_5c_{(2+3+4)}\right) - l_5c_1c_5 \\ &r_{31} = s_{(2+3+4)}c_5, r_{32} = -s_{(2+3+4)}s_5, r_{33} = c_{(2+3+4)}, r_{34} = l_5s_{(2+3+4)}c_5 \\ &r_{14} = r_{24} = r_{34} = 0, r_{44} = 1 \end{aligned} \quad (5)$$

In the expressions of Equation 5, the variables are defined by Equation 6 as:

$$c_i = cos\,\theta_i,\ \ s_i = sin\,\theta_i\,,\ c_{ij} = cos\left(\theta_i + \theta_j\right),\ s_{ij} = sin(\theta_i + \theta_j) \quad (6)$$

By using the T-matrix, it is possible to calculate the values of (P_x, P_y, P_z) with respect to the fixed coordinate system. Then, the P_x, P_y and P_z obtained with direct kinematics are expressed as shown in Equation 7 as:

$$\begin{aligned} P_x = {} & cos\,\theta_1\,[l_1 + l_2\,cos\,\theta_2 + l_3\,cos(\theta_2 + \theta_3) + l_4\,cos(\theta_2 + \theta_3 + \theta_4) + \\ & l_5\,cos\,\theta_5\,cos(\theta_2 + \theta_3 + \theta_4)] + l_5sin\,\theta_1\,sin\,\theta_5] \\ P_y = {} & sin\,\theta_1\,[l_1 + l_2\,cos\,\theta_2 + l_3\,cos(\theta_2 + \theta_3) + l_4\,cos(\theta_2 + \theta_3 + \theta_4) + \\ & l_5\,cos\,\theta_5\,cos(\theta_2 + \theta_3 + \theta_4)] - l_5cos\,\theta_1\,sin\,\theta_5] \\ P_z = {} & l_2\,sin\,\theta_2 + l_3\,sin(\theta_2 + \theta_3) + l_4\,sin(\theta_2 + \theta_3 + \theta_4) + l_5\,cos\,\theta_5\,sin(\theta_2 + \theta_3 + \theta_4) \end{aligned} \quad (7)$$

The orientation of RAVebots-1 end-effector in space can be described by attaching a coordinate system to it and then describing the vector of its coordinate axes relative to reference frame. Figure 6 indicates the normal vector ($\vec{n}$), orientation vector ($\vec{o}$), approach vector ($\vec{a}$) and the resultant of all vectors ($\vec{D}$) of the end-effector which described in more detail in Equation 8.

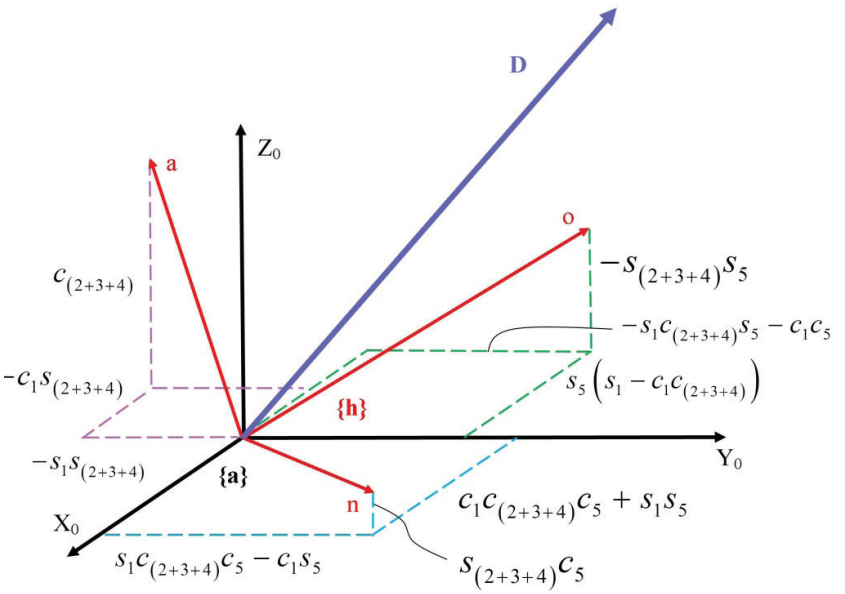

Figure 6- Rotation matrix elements

$$\vec{n} = \begin{bmatrix} c_1c_{(2+3+4)}c_5 + s_1s_5 \\ s_1c_{(2+3+4)}c_5 - c_1s_5 \\ s_{(2+3+4)}c_5 \end{bmatrix}, \vec{o} = \begin{bmatrix} s_5\left(s_1 - c_1c_{(2+3+4)}\right) \\ -s_1c_{(2+3+4)}s_5 - c_1c_5 \\ -s_{(2+3+4)}s_5 \end{bmatrix}, \vec{a} = \begin{bmatrix} -c_1s_{(2+3+4)} \\ -s_1s_{(2+3+4)} \\ c_{(2+3+4)} \end{bmatrix},$$

$$\vec{D} = (\vec{n} + \vec{o}) + \vec{a} = \begin{bmatrix} c_1\left(c_{(2+3+4)}(c_5 - s_5) - s_{(2+3+4)}\right) + 2s_1s_5 \\ s_1\left(c_{(2+3+4)}(c_5 - s_5) - s_{(2+3+4)}\right) + c_1c_4 \\ s_{(2+3+4)}(c_5 - s_5) + c_{(2+3+4)} \end{bmatrix} \quad (8)$$

2.3.2. Inverse kinematics

The conversion of the position and orientation of the manipulator's end-effector from Cartesian space to joint space is known as inverse kinematics. The inverse kinematics solution uses the position and orientation (p_x, p_y, p_z) of the robot's end-effector, which has been known to solve the joint angles (θ_1, θ_2, θ_3, θ_4, θ_5). In this study, the geometrical method was used.

In the RAVebots-1, the axes of the last two joints intersect at one point, which is referred to as point A. The position of point A is independent of the two joints of θ_4, and θ_5. Therefore, only the three previous joints should be considered when solving the position of point A. The position of point A is denoted as $P_a = [P_{ax}, P_{ay}, P_{az}]$ which showed by Equation 9.

$$P_{ax} = P_x - P_{x_5}^3, \; P_{ay} = P_y - P_{y_5}^3, \; P_{az} = P_z - P_{z_5}^3 \quad (9)$$

I. Solutions of the arm joint angles (θ_1, θ_2, θ_3).

The position of point A can be determined from the homogeneous transformation matrix, which is derived from T_1^0, T_2^1, T_3^2 as shown in Equation 10.

$$T_3^0 = \prod_{i=1}^{3} T_i^{i-1} = T_1^0 T_2^1 T_3^2$$

$$= \begin{bmatrix} c_1c_{23} & -c_1s_{23} & s_1 & c_1(l_3c_{23} + l_2c_2 + l_1) \\ s_1c_{23} & -s_1s_{23} & -c_1 & s_1(l_3c_{23} + l_2c_2 + l_1) \\ s_{23} & c_{23} & 0 & l_3s_{23} + l_2s_2 \\ 0 & 0 & 0 & 1 \end{bmatrix} \quad (10)$$

Elements of P_a can be described by Equation 11.

$$P_{ax} = c_1(l_3c_{23} + l_2c_2 + l_1), P_{ay} = s_1(l_3c_{23} + l_2c_2 + l_1), P_{az} = l_3s_{23} + l_2s_2 \quad (11)$$

From Equation 11, it is possible to obtain Equation 12 as:

$$\frac{P_{ay}}{P_{ax}} = \frac{s_1}{c_1} \rightarrow \theta_1 = Atan\,2(P_{ay}, P_{ax}) \quad (12)$$

From Equation 11, it is possible to obtain Equation 13.

$$P_{ax}.c_1 + P_{ay}.s_1 = ({c_1}^2 + {s_1}^2)(l_3c_{23} + l_2c_2 + l_1) = l_3c_{23} + l_2c_2 + l_1 = A \quad (13)$$

In the RAVebots-1, c_{23} can be obtained from Equation 12 as follows:

$$c_{23} = \frac{(P_{ax}.c_1 + P_{ay}.s_1) - l_2c_2 - l_1}{l_3} \quad (14)$$

It is possible to obtain s_{23} by solving Equation 11 as follows:

$$s_{23} = \frac{P_{az} + l_2s_2}{l_3} \quad (15)$$

Substituting Equation 14 and Equation 15 into the equation ${c_{23}}^2 + {s_{23}}^2 = 1$ yields Equation 16.

$$\left((P_{ax}.c_1 + P_{ay}.s_1 - l_1) - l_2c_2\right)^2 + (P_{az} + l_2s_2)^2 = {l_3}^2$$

$$P_{az}s_2 + (P_{ax}.c_1 + P_{ay}.s_1 - l_1)c_2 = \frac{(P_{ax}.c_1 + P_{ay}.s_1 - l_1)^2 + {l_2}^2 + {P_{az}}^2 - {l_3}^2}{2l_2} = A \quad (16)$$

Consider the variables *d*, *f*, and *g* as defined in Equation 17.

$$d = P_{az};\ f = P_{ax}.c_1 + P_{ay}.s_1 - l_1;\ g = \frac{(P_{ax}.c_1 + P_{ay}.s_1 - l_1)^2 + {l_2}^2 + {P_{az}}^2 - {l_3}^2}{2l_2} \quad (17)$$

Replacing the variables from Equation 17 in Equation 16 yields Equation 18:

$$d\,sin\,\theta_2 + f cos\theta_2 = g \quad (18)$$

Considering the approximations shown in Equation 19.

$$\begin{aligned} &f+g\neq 0, \qquad d\sqrt{d^2+f^2-g^2}-d^2-f^2-fg\neq 0 \;\rightarrow \theta_2 \\ &\approx 2.\left(3.14159\,n+tan^{-1}\left(\frac{d-\sqrt{d^2+f^2-g^2}}{f+g}\right)\right), n\in z \\ &f+g\neq 0, \qquad d\sqrt{d^2+f^2-g^2}+d^2+f^2+fg\neq 0 \;\rightarrow \theta_2 \\ &\approx 2.\left(3.14159\,n+tan^{-1}\left(\frac{d+\sqrt{d^2+f^2-g^2}}{f+g}\right)\right), n\in z \end{aligned} \tag{19}$$

$$d\neq 0,\ d^2+f^2\neq 0\,, g\approx -f\rightarrow \theta_2\approx 2.\left(3.14159\,n+tan^{-1}\left(\frac{f}{d}\right)\right), n\in z$$

$$g=-f\ \rightarrow \theta_2=2\pi n+\pi, n\in z$$

And if g= -f, x=$2n\pi$+π it is possible to obtain Equation 20.

$$\begin{aligned} \theta_2 &= Atan\,2\left(\frac{fg-\sqrt{d^4+d^2f^2-d^2g^2}}{d^2+f^2},\frac{1}{d}\left(\frac{f\sqrt{-d^2(-d^2-f^2+g^2)}-f^2g}{d^2+f^2}+g\right)\right) \\ \theta_2 &= Atan\,2\left(\frac{fg+\sqrt{d^4+d^2f^2-d^2g^2}}{d^2+f^2},\frac{1}{d}\left(\frac{-f\sqrt{-d^2(-d^2-f^2+g^2)}-f^2g}{d^2+f^2}+g\right)\right) \end{aligned} \tag{20}$$

The result of using Equation 14 and 15 yields Equation 21.

$$tan(\theta_2+\theta_3)=\frac{P_{az}+l_2s_2}{(P_{ax}.c_1+P_{ay}.s_1)-l_2c_2-l_1} \tag{21}$$

It is possible to solve Equation 21 as shown in Equation 22.

$$\theta_3=Atan\,2\left(P_{az}+l_2s_2,\ (P_{ax}.c_1+P_{ay}.s_1)-l_2c_2-l_1\right)-\theta_2 \tag{22}$$

II. Solutions of the wrist joint angles *(θ_4 and θ_5)*.

The orientation of the robot is controlled by the rotation matrix, and the orientation of A is described by T_3^0. The orientation of end-effector is described by T_5^0. The relationship between T_3^0 and T_5^0 is $T_5^0=T_3^0\,T_5^3$. Matrix T_5^3 can be described as shown in Equation 23.

$$T_5^3=\prod_{i=3}^{5}T_i^{i-1}=T_4^3\,T_5^4=\begin{bmatrix} c_4c_5 & -c_4s_5 & -s_4 & (l_5c_5+l_4)c_4 \\ s_4c_5 & -s_4s_5 & c_4 & (l_5c_5+l_4)s_4 \\ s_5 & c_5 & 0 & l_5s_5 \\ 0 & 0 & 0 & 1 \end{bmatrix} \tag{23}$$

The elements of $P_{A_5}^{\ 3}$ come from the fourth column of the 4×4 matrix in Equation 23, which can be described by Equation 24.

$$P_{x_5}^{\ 3}=(l_5c_5+l_4)c_4,\ \ P_{y_5}^{\ 3}=(l_5c_5+l_4)s_4,\ \ P_{z_5}^{\ 3}=l_5s_5 \tag{24}$$

From Equation 24, it is possible to obtain Equation 25 as:

$$\frac{P_{y_5}^{\ 3}}{P_{x_5}^{\ 3}} = \frac{s_4}{c_4} \rightarrow \theta_4 = Atan\,2\left(P_{y_5}^{\ 3}, P_{x_5}^{\ 3}\right) \quad (25)$$

Also, Equation 25 yields Equation 26 and Equation 27.

$$sin\,\theta_5 = \frac{P_{z_5}^{\ 3}}{l_5} \quad (26)$$

$$cos\,\theta_5 = \frac{P_{x_5}^{\ 3} - l_4 c_4}{l_5 c_4} \quad (27)$$

Then from Equation 26 and Equation 27, it is possible to obtain Equation 28.

$$\theta_5 = Atan\,2\left(\frac{P_{z_5}^{\ 3}}{l_5}, \frac{P_{x_5}^{\ 3} - l_4 c_4}{l_5 c_4}\right) \quad (28)$$

3. Results and Discussion

3.1. Torque calculation

Table 2 presents the results of torque calculation explained in Equation 1. In agricultural robots, the speed is of secondary importance. The servo motor's speeds of RAVebots-1 is set to 15 rpm in J_1 and 60 rpm in J_5. Above this speed values, $T_{Dynamic}$ and the inertia increase dramatically. A bigger $T_{Dynamic}$ requires a more powerful power supply in order to control the servo motors. The T_{Static} in J_1 and J_5 is zero, because in the designing process the angle between the total force vector and the perpendicular length from pivot to force is 90°. In other words, the direction of the total force vector is not in the rotation direction. In general, because of the rotation speed, $T_{Dynamic}$ in each joint is not zero. Also, in J_2, J_3 and J_4, T_{Static} is bigger than $T_{Dynamic}$. It is shown, that the effect of T_{Static} is greater than $T_{Dynamic}$. As a conclusion, J_2 needs the most powerful servo motor for the highest torque, and J_5 needs the weakest one.

Table 2- Maximum joints specification in C design

Joint	*Speed (rpm)*	T_{Static} $(N.m)$	$T_{Dynamic}$ $(N.m)$	T_{Total} $(N.m)$	$T_{Total\ (include\ FOS)}$ $(N.m)$
J_1	15	0	5.15	6.15	18.5 (FOS= 3)
J_2	30	253	4.35	257.35	287.3 (FOS= 1.1)
J_3	30	101.9	1.5	103.4	173.5 (FOS= 1.7)
J_4	30	20.1	0.1	20.2	32.9 (FOS= 1.6)
J_5	60	0	0.1	0.1	0.2 (FOS= 2)

The results of the dynamic simulation in SOLIDWORKS showed in Figures 7 and 8 for joints 2 and 3, respectively. It can be seen that the value of total torque is not stable. According to Figure 7, the total torque value varies between 209.5 N.m and -30.2 N.m, and in Figure 8 this parameter changes in the range of 83.3 to 134.3 N.m. Therefore, this erratic parameter requires a logical *FOS* (Factor of Safety). In order to cover unpredictable circumstances like impact and fluctuation, in all design calculations, *FOS* was considered between 1.1 and 2.

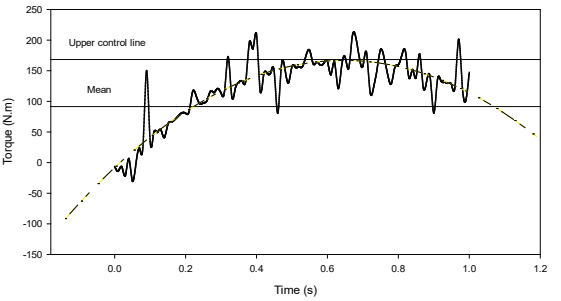

Figure 7- Torque calculation of Joint 2

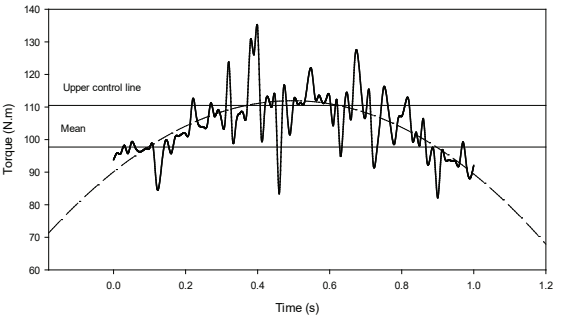

Figure 8- Torque calculation of Joint 3

3.2. The effect of material changes in the required torque

Table 3 illustrates the values of required torque in three different types of conditions (material and servo motor location) for the RAVebots-1. It is evident that the static, dynamic and total torque declines in different conditions, whereas the robot fundamental structure, remained unchanged. In condition A which is the reference condition, all the components were designed

and manufactured by using ASTM A36 steel and all servo motors were installed on their respective joint position. It means that the servo motor number 2 is set in the joint 2, the servo motor number 3 is set in the joint 3, and so on. In condition B, the components material was changed to AL5202. In condition C, not only the component materials were changed to AL5202 but also the positions of servomotors were improved. As shown in Figure 9, all torque values were reduced dramatically from condition A to C. It can be seen that the total torque in J_1, J_2, J_3 and J_4 was reduced from condition A to B due to the change of material. There is no rule for decreasing static torque because of the complex structure of the body. Also, the material changes were done on the main body components, and the joints, bolts and nuts material remained the same. The position of the servo motors changed for the conditions C; giving as a result reductions of total torque in J_1, J_2 and J_3 joints. Because of the RAVebots-1 special structure, the static torque in J_1 and J_5 is equal to zero for all conditions. As a conclusion, adjusting the material of the body and the servo motor location directly affects the torque values.

Table 3- Effect of linkage material changing and servo motor position improving joints torque

Condition	*Torque (N.m)*	I_1	I_2	I_3	I_4	I_5
A	Static	0	634	233.5	33.1	0
	Dynamic	14.48	14	3.1	0.17	0
	Total	15.48	648	236.6	33.27	0
B	Static	0	360.5	134.25	20.1	0
	Dynamic	7.57	8.5	1.95	0.1	0.1
	Total	8.57	369	136.20	20.2	0.1
C	Static	0	253	101.9	20.1	0
	Dynamic	5.15	4.35	1.5	0.1	0.1
	Total	6.15	257.35	103.4	20.2	0.1

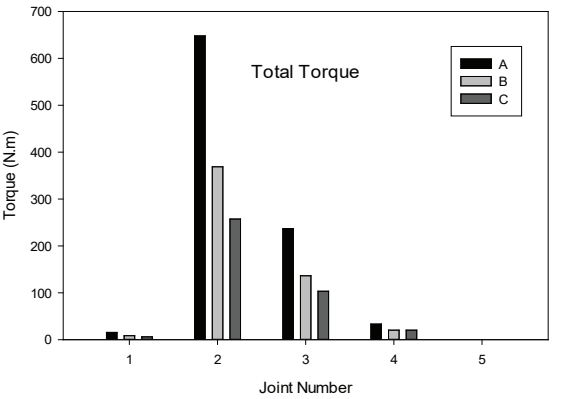

Figure 9- The impact of changing the type of material and the joint position in the total torque

3.3. Validation of forward kinematics

The length of the body links was I_1 = 484 mm; I_2 = 650 mm; I_3 = 600 mm; I_4 = 250 mm and I_5 = 250 mm. The forward kinematics can be used to find the end-effector coordinate of the robot movement by substituting the constant parameters values in Equation 7. The final equation of the end-effector's envelopment for the D-H convention of forward kinematics is listed as follows:

$$\begin{aligned} P_x &= \cos\theta_1\,[0.484 + 0.65\cos\theta_2 + 0.6\cos(\theta_2+\theta_3) + 0.25\cos(\theta_2+\theta_3+\theta_4) + \\ &\quad 0.25\cos\theta_5\cos(\theta_2+\theta_3+\theta_4)] + 0.25\sin\theta_1\sin\theta_5] \\ P_y &= \sin\theta_1\,[0.484 + 0.65\cos\theta_2 + 0.6\cos(\theta_2+\theta_3) + 0.25\cos(\theta_2+\theta_3+\theta_4) + \\ &\quad 0.25\cos\theta_5\cos(\theta_2+\theta_3+\theta_4)] - 0.25\cos\theta_1\sin\theta_5] \\ P_z &= 0.65\sin\theta_2 + 0.6\sin(\theta_2+\theta_3) + 0.25\sin(\theta_2+\theta_3+\theta_4) + \\ &\quad 0.25\cos\theta_5\sin(\theta_2+\theta_3+\theta_4) \end{aligned} \quad (29)$$

In the zero position, the orientation vectors are defined as follows in Equation 30.

$$Zero\ position \xrightarrow{\forall\theta_i,\ 1\le i\le 5,\ \theta_i=0} \vec{n} = \begin{bmatrix}1\\0\\0\end{bmatrix}, \vec{o} = \begin{bmatrix}0\\-1\\0\end{bmatrix}, \vec{a} = \begin{bmatrix}0\\0\\1\end{bmatrix}, \vec{D} = \begin{bmatrix}0\\0\\1\end{bmatrix} \quad (30)$$

Generally, the direction of the orientation vectors in the zero position proves the algorithm validity. It means, in the zero position, the normal vector ($\vec{n}$), the orientation vector ($\vec{o}$) and the approach vector ($\vec{a}$) have to be in the same direction of the axes *X*, *-Y* and *Z,* respectively. Therefore, all of the coordinate frames in Figure 5 were removed except the base, which is the reference coordinate frame for determining the link parameters in zero position. The zero position is necessary to choose a home position. The home position is the initial position of the arm and it can be any arbitrary position within the workspace. However, it is better to have a defined home position as a reference point to start the algorithm run.

4. Conclusions

Based on experimental results, one can conclude the factors that affected arm performance in the mentioned robotic design are the selection of material, torque optimization analysis (utilizing appropriate techniques), selecting optimized algorithms, and using adequate speed control for servo motors. Addressing design challenges and working through such challenges provides the opportunity to achieve the best possible produce. Findings based on experimental results are summarized below:

1. The results of kinematic calculation show that the final developed algorithm worked effectively. The presented algorithm establishes a smooth curve to move and reach the target point rapidly.
2. The presented strategy for material improvement and heavy components modification has positive results on maximum payload, mass center position, and total components weight. Also, it improved the servo motor's required torque more effectively. The Solidworks simulation results and the detailed mass effect on required torque for situation A, B, and C confirm this conclusion.
3. In the mentioned rotation speed for each join, the results show that RAVebots-1's reaction velocity varies from 1.18 to 1.68. This is the velocity between a specified home position and the maximum front position, located in 1640 mm from the main joint.
4. According to the RAVebots-1 workspace simulation, it is possible to expand the robot arm application for horticulture usage e.g. fruit picking, cutting the tree branches, cover the fruits and precision spraying.

Hopefully, in the future, the RAVebots-1 design will be produced and utilized in everyday agricultural practices, especially for harvesting heavy crops, as well as picking other crops. This robotic arm will be capable of harvesting by using a camera and a specially designed end-effector. The robot will be capable of collecting physical data of the crops (weight, volume, density, etc.), harvesting crops, and then depositing the crops into a designated location

Acknowledgements

This study was supported by the Cross-ministerial Strategic Innovation Promotion Program (SIP) managed by Cabinet Office.

References

Angeles J (1997). Fundamentals of Robotic Mechanical Systems. Theory, Methods and Algorithms. Springer, New York

Balkan T, Özgören M K, Sahir Arıkan M A & Baykurt H M (2000). A method of inverse kinematics solution including singular and multiple configurations for a class of robotic manipulators. *Mechanism and Machine Theory* **35**(9): 1221-1237

Barawid Jr O C, Mizushima A, Ishii K & Noguchi N (2007). Development of an Autonomous Navigation System using a Two-dimensional Laser Scanner in an Orchard Application. *Biosystems Engineering* **96**(2): 139-149

Cassinis R & Tampalini F (2007). AMIRoLoS an active marker internet-based robot localization system. *Robotics and Autonomous Systems* **55**(4): 306-315

Craig J J (1989). Introduction to Robotics Mechanics and Control. USA:Addision-Wesley Publishing Company

De-An Z, Jidong L, Wei J, Ying Z & Yu C (2011). Design and control of an apple harvesting robot. *Biosystems Engineering* **110**(2): 112-122

Denavit J & Hartenberg R S (1955). A kinematic notation for lower-pair mechanisms based on matrices. *Journal of Applied Mechanics* **1**: 215-221

Funda J, Taylor R H & Paul R P (1990). On homogeneous transforms, quaternions, and computational efficiency. *IEEE Transactions on Robotics and Automation* **6**: 382-388

Ghazvini M (1993). Reducing the inverse kinematics of manipulators to the solution of a generalized eigenproblem. In: J Angeles, G Hommel, Kovács (Eds), *Computational Kinematics, Solid Mechanics and its Applications* **28**: 15-26

Hayashi S, Shigematsu K, Yamamoto S, Kobayashi K, Kohno Y, Kamata J & Kurita M (2010). Evaluation of a strawberry-harvesting robot in a field test. *Biosystems Engineering* **105**(2): 160-171

Karlik B & Aydin S (2000). An improved approach to the solution of inverse kinematics problems for robot manipulators. *Engineering Applications of Artificial Intelligence* **13**(2): 159-164

Kondo N, Monta M & Fujiura T (1996). Fruit harvesting robots in Japan. *Advances in Space Research* **18**(1-2): 181-184

Lee H-Y & Liang C-G (1988). Displacement analysis of the general spatial 7-link 7R mechanism. *Mechanism and Machine Theory* **23**(3): 219-226

MAFF (2016). TPP or no, aging farm sector needs true reform. [Online] Available: http://www.maff.go.jp/e/index.html.

Raghavan M & Roth B (1990). Inverse kinematics of the general 6R manipulator and related linkages. Transactions of the ASME, *Journal of Mechanical Design* **115**: 228-235

Richard B & Keith N (2006). Shigley's Mechanical Engineering Design. McGraw-Hill Publishing Company

Satoru G (2011). ROBOT ARMS. InTech publisher, ISBN 978-953-307-160-2

Serdar K & Zafer B (2006). Industrial robotics theory modelling and control. Pages 964 in C. Sam, ed

Siciliano B & Khatib O (2008). Handbook of Robotics, Springer publisher, ISBN 978-3-540-23957-4

Tanigaki K, Fujiura T, Akase A & Imagawa J (2008). Cherry-harvesting robot. *Computers and Electronics in Agriculture* **63**(1): 65-72

Tanner H G, Kyriakopoulos K J & Krikelis N I (2001). Advanced agricultural robots: kinematics and dynamics of multiple mobile manipulators handling non-rigid material. *Computers and Electronics in Agriculture* **31**(1): 91-105

USDA (2015). Farm Demographics - U.S. Farmers by Gender, Age, Race, Ethnicity, and More, United States Department of Agricultur (onile article), https://www.agcensus.usda.gov/Publications/2012/Online_Resources/Highlights/Farm_Demographics

Wang S-C, Hikita H, Kubo H, Zhao Y-S, Huang Z & Ifukube T (2003). Kinematics and dynamics of a 6 degree-of-freedom fully parallel manipulator with elastic joints. *Mechanism and Machine Theory* **38**(5): 439-461

Yahya S, Moghavvemi M & Mohamed H A F (2011). Geometrical approach of planar hyper-redundant manipulators: Inverse kinematics, path planning and workspace. *Simulation Modelling Practice and Theory* **19**(1): 406-422

Zion B, Mann M, Levin D, Shilo A, Rubinstein D & Shmulevich I (2014). Harvest-order planning for a multiarm robotic harvester. *Computers and Electronics in Agriculture* **103**: 75-81